

# We are IntechOpen, the world's leading publisher of Open Access books Built by scientists, for scientists

6,900

Open access books available

185,000

International authors and editors

200M

Downloads

Our authors are among the

154

Countries delivered to

TOP 1%

most cited scientists

12.2%

Contributors from top 500 universities



WEB OF SCIENCE™

Selection of our books indexed in the Book Citation Index  
in Web of Science™ Core Collection (BKCI)

Interested in publishing with us?  
Contact [book.department@intechopen.com](mailto:book.department@intechopen.com)

Numbers displayed above are based on latest data collected.  
For more information visit [www.intechopen.com](http://www.intechopen.com)



---

# Metasurfaces for Spatial Light Manipulation

---

Jian Wang and Jing Du

Additional information is available at the end of the chapter

<http://dx.doi.org/10.5772/66319>

---

## Abstract

Light manipulation means that one can take advantages of different physical dimensions of lightwaves to realize flexible light control. Light manipulation over subwavelength propagation distances can be realized using metasurfaces. There are two categories of metasurfaces divided by the material type of unit structure, that is, plasmonic and dielectric metasurfaces. For plasmonic metasurfaces, they are made on the basis of metallic meta-atom whose optical responses are driven by the plasmon resonances supported by metallic particles. For dielectric metasurfaces, unit structure is constructed with high refractive index dielectric resonators such as silicon, germanium, or tellurium, which can support electric and magnetic dipole responses based on Mie resonances. The responses of plasmonic and dielectric metasurfaces are all relevant to the characteristics of unit structure. One can manipulate the electromagnetic field of lightwave scattered by the metasurfaces through designing the dimension parameters of each unit structure in the metasurfaces. In this chapter, we review our recent research progress in light manipulation using plasmonic and dielectric metasurfaces. It is believed that metasurfaces based nanophotonic devices are one of the most potential devices applied in various fields such as beam steering, spatial light modulator, nanoscale-resolution imaging, sensing, quantum optics devices, and even optical communication networks.

**Keywords:** light manipulation, metamaterials, metasurfaces, plasmonic metasurfaces, dielectric metasurfaces, orbital angular momentum, vector beams, Bessel beams, space-division multiplexing

---

## 1. Introduction

The fundamental properties of lightwaves can be described from the basic electrical field expression of electromagnetic waves,  $E(x, y, z, t) = e(z, t) \cdot F(x, y, t) \cdot |A(z, t)| \cdot \Phi(z, t) \cdot \exp$

---

$[j(\omega t - kz) + \varphi]$ , as displayed in **Figure 1**, where  $\vec{e}(z, t)$  is the polarization,  $F(x, y, t)$  is related to the spatial structure,  $|A(z, t)|$  is the amplitude,  $\Phi(z, t)$  is the phase,  $A(z, t) = |A(z, t)| \cdot \Phi(z, t)$  is the complex amplitude,  $\omega$  is the frequency of the lightwave,  $k$  is the wave vector,  $\varphi$  is the initial phase,  $z$  is the propagation distance and  $t$  is the time [1]. Light manipulation means that one can take advantages of these physical dimensions (wavelength/frequency, time, complex amplitude, polarization, spatial structure) of lightwaves to realize flexible control of electromagnetic waves. Utilizing different physical dimensions of lightwaves, light manipulation has been widely applied in various areas such as wavelength-division multiplexing (WDM) [2], polarization-division multiplexing (PDM) [3], time-division multiplexing (TDM) [4], space-division multiplexing (SDM) [5], advanced modulation format [6], sensing [7], imaging [8], optical tweezers [9], optical knots [10], optical trapping [11], and so on. In order to realize light manipulation on the physical dimensions of lightwaves, there have been lots of approaches such as modulators (e.g. intensity, phase, I/Q modulators, spatial light modulators, etc.), conventional optical elements (e.g. lens, waveplate, polarizer, optical coupler, etc.), and metamaterials and metasurfaces, as listed in **Figure 2** [4–11]. The spatial structure physical dimension has recently attracted increasing interest in wide research areas. In this chapter, we mainly focus on the recent progress in light manipulation on spatial structure physical dimension using metasurfaces.

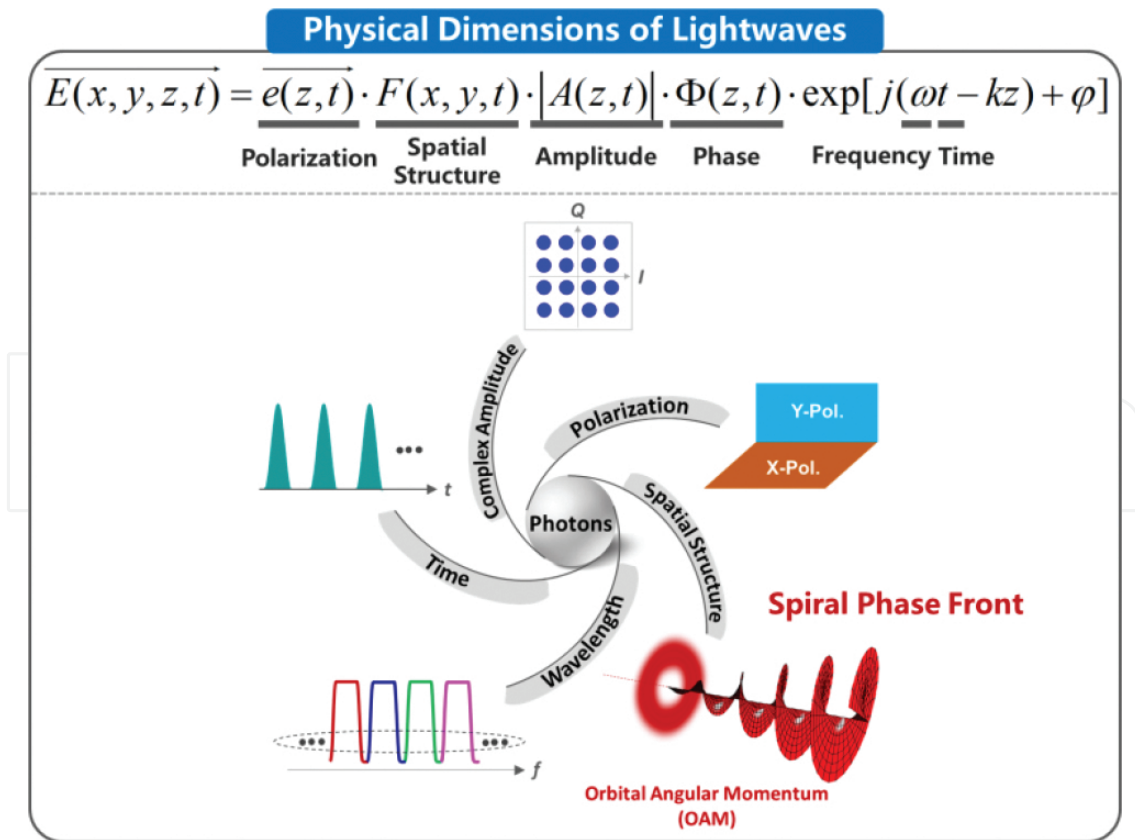


**Figure 1.** Schematic illustration of physical dimensions of lightwaves.

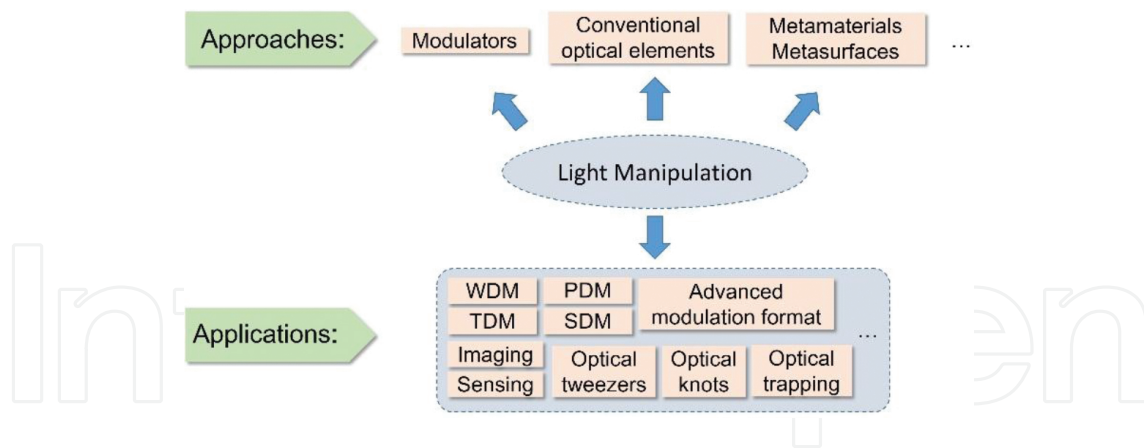


**Figure 2.** Schematic illustration of approaches and applications of light manipulation.

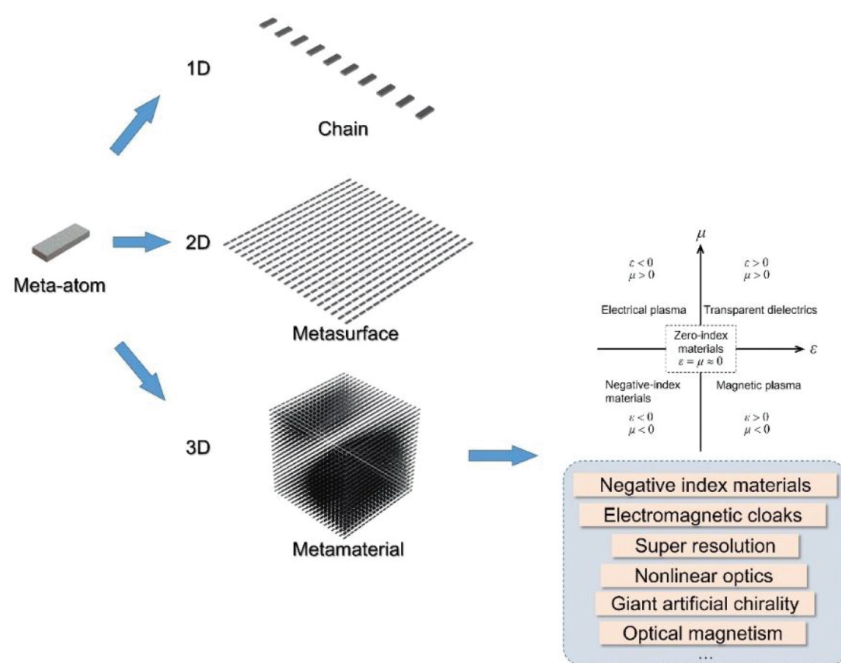


**Figure 3.** Schematic illustration of meta-atom, 1D chain, 2D metasurface, and 3D metamaterial. Inserts are the representation of the parameter space for permittivity  $\epsilon$  and permeability  $\mu$  and the typical examples of applications of metamaterials.

“Metamaterial” can be defined as a man-made material whose properties can be attained by designing the unit structure. It has been widely focused for a dozen years since it was firstly reported by Smith et al. in 2000 [12]. The unit structure in metamaterial called as meta-atoms or meta-molecules, must be considerably smaller than the operating wavelength, and the distance between neighboring meta-atoms also has subwavelength scale [13]. This subwavelength scale in homogeneity makes the whole metamaterial uniform on the macro of performance, and this phenomenon makes this artificial structure essentially a “material” rather than a device. Therefore, one can arbitrarily arrange the so-called meta-atoms into periodic arrays to build one-dimensional (1D) materials (chains), two-dimensional (2D) materials (metasur-

faces), and three-dimensional (3D) materials (metamaterials), as shown in **Figure 3** [14]. For metamaterial, one can even manipulate its macroscopical properties such as permittivity  $\epsilon$  and permeability  $\mu$ . The researches of metamaterial are essentially related to the exploitation of the electromagnetic parameter space for better control of electromagnetic waves, as depicted in **Figure 3**. Utilizing metamaterials, one can enter regions of the electromagnetic parameter space that are not observed in conventional material but are not forbidden by Maxwell's equations such as third quadrant of the parameter space (negative-index materials), zero-index materials and space far away from the non-magnetic line [15]. Taking advantage of these attractive features, as shown in **Figure 1**, metamaterials have been widely applied in optical negative index materials [16], nonlinear optics [17], optical magnetism [18], super resolution [19], giant artificial chirality [20], electromagnetic cloaks [21], and so on.

Besides 3D materials, 2D metasurfaces are also widely focused for their ability of flexible light manipulation (phase, amplitude, polarization) over subwavelength propagation distances [22]. Most of the metasurfaces can be divided into two categories by the material type of unit structure: plasmonic and dielectric, as displayed in **Figure 4**. For plasmonic metasurfaces, they are made on the basis of metallic meta-atom whose optical responses are driven by the plasmon resonances supported by metallic particles. When a metallic particle is placed in an electric field, the conduction electrons are escaped from their equilibrium positions with respect to the core ions, resulting in a polarization of the particle and generating a depolarizing field. In a time-varying external field, this collective motion in the metallic particle can be seen as a Lorentzian oscillator whose characteristic peak in the displacement amplitude is around the resonance frequency and accompanied by a phase shift of  $\pi$  over the spectral width of the resonance [14]. For dielectric metasurfaces, unit structure is constructed with high refractive index dielectric resonators such as silicon, germanium or tellurium, which can support electric and magnetic dipole responses based on Mie resonances [23]. When a dielectric particle is illuminated by a light wave whose frequency is below or near the bandgap frequency of the material of particle, both the magnetic dipole (first Mie resonance) and electric dipole resonances (second Mie resonance) are excited. The magnetic and electric Mie resonance can then enhance the magnetic and electric field at the particle's center at optical frequencies, respectively, and this enhancement is related to the intrinsic properties of dielectric particles [24]. Therefore, the responses of plasmonic and dielectric metasurfaces are all relevant to the characteristics of unit structure such as dimensions and materials. One can manipulate the electromagnetic field of light wave scattered by the metasurfaces through designing the dimension parameters of each unit structure in the metasurfaces [25].

To produce the designed metasurfaces, many attractive previous works have reported the fabrication techniques such as electron-beam lithography [16], focused-ion beam [26], interference lithography [27], and nanoimprint lithography [28]. Electron-beam lithography is a standard method that can fabricate the metasurface with high nanoscale resolution. Focused-ion beam is a more appropriate method for rapid prototyping. Interference lithography can provide a solution for realizing large-scaled metasurface fabrication. Nanoimprint lithography is a more promising technique for combining many advantages of the formers such as high-resolution, large-scaled producing, and low processing cost [28, 29]. The unique properties

and the development of fabrication techniques have made metasurfaces applied in various fields such as flat optics [30–41], nonlinear effects [42, 43], photonic Hall effects [44], electromagnetically induced transparency [45], cloaking [46], and so on as shown in **Figure 4**. For instance, the applications of metasurfaces in the field of flat optics mainly include anomalous wave plates [30], reflection/refraction [31, 32], flats lens/axicons [33], mirrors [35], hologram [37], filters [38], optical vortex generation [39, 40], polarization beam splitter [41], and so on. The applications of metasurfaces in the field of nonlinear effects mainly include second/third harmonic generation [42] and enhanced absorbing [43].

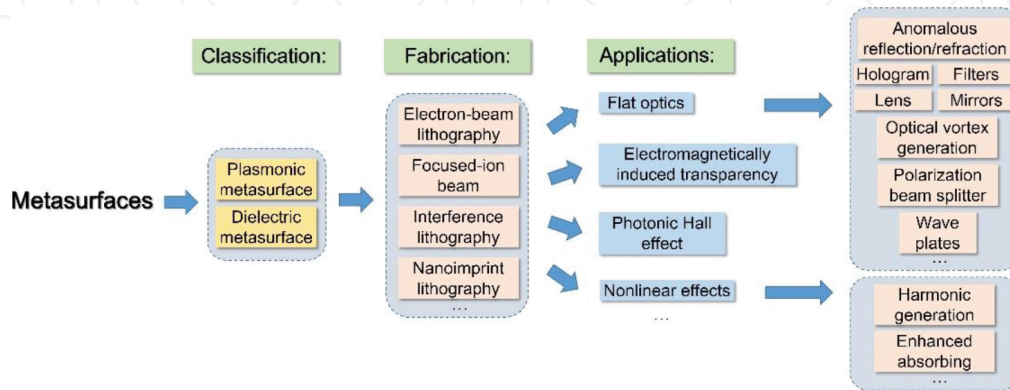


**Figure 4.** Schematic illustration of classification, fabrication and applications of metasurfaces.

In this review article, we go over our recent progress in light manipulation using plasmonic and dielectric metasurfaces, including metasurfaces-based broadband and selective generation of orbital angular momentum (OAM)-carrying vector beams [47, 48], N-fold OAM multicasting using V-shaped antenna array [49], metasurface on conventional optical fiber facet for linearly polarized mode (LP11) generation [50], OAM beams generation using nanophotonic dielectric metasurface array [51], and Bessel beams generation and OAM multicasting using dielectric metasurface array [52].

## 2. Light manipulation using plasmonic metasurfaces

Plasmonic metasurfaces are composed of metal nanoparticles based on the plasmon resonances. Several typical types of plasmonic metasurfaces and previous works are reported: (1) metal V-shaped nanoantennas are designed and fabricated on silicon substrate using electron-beam lithography method to manipulate the phase of scattering light and generate OAM beams [22]; (2) Au patch antennas separated from a metal back plane by a MgF<sub>2</sub> spacer are designed and fabricated using electron-beam evaporation electron-beam lithography technique to realize anomalous reflections [31]; (3) metal H-shaped nanoantenna arrays are designed and fabricated using printed circuit boards to realize high efficiency conversion from propagating waves to surface waves in microwave regime [32]; (4) metal nanorods are deposited on the glass substrate to generate hologram [37]; (5) freestanding nanofabricated fishnet metasurfaces are

designed and fabricated using electron-beam lithography method to realize broadband band pass filter [38]; (6) metal rectangular apertures are arranged into an array with rotational symmetry in metal film to generate OAM beams [39]; (7) metal nanorods are designed and fabricated on glass substrate with a standard electron-beam lithography and lift-off process to generate broadband OAM beams [40]; (8) metal split-ring resonators are designed and fabricated on glass substrate with a standard electron-beam lithography to enhance second harmonic generation [42]. All these works are based on manipulating the plasmon responses of nanoresonators by altering the dimensions, directions and even arrangement of unit structures. Recently, we have also made some progresses in plasmonic metasurfaces on the basis of previous works.

### 2.1. Metasurfaces-based broadband and selective generation of OAM-carrying vector beams [47, 48]

We propose and design compact metal-assisted metasurfaces to enable broadband generation of OAM-carrying vector beams. **Figure 5(a)** and **(b)** depicts the structure and geometric parameters of metal-assisted metasurfaces. We design two concentric rings in a gold film with a thickness of  $h = 200$  nm. Each ring is composed of 42 rectangular apertures with gradually varied orientation. The rectangular aperture array in the gold film can enhance the transmission of linearly polarized light (perpendicular to the aperture direction), which might be explained as follows: (1) the localized waveguide resonance (each air aperture can be regarded as a truncated rectangular waveguide with four metal walls and two sides open to air); (2) the property of the surface plasmon resonance due to the aperture array. Hence, each rectangular aperture can be regarded as a localized linear polarizer. By controlling the orientation angle of rectangular apertures, we can construct desired spatially variant polarizers to generate OAM-carrying vector beams with right or left circularly polarized input light beam. **Figure 5(c)** shows an example of phasefront and spatial polarization after passing through the metasurfaces, which indicates the generation of OAM-carrying vector beam from circularly polarized beam.

**Figure 6** plots spatial phase, power and polarization distributions of output beams under the excitation of input left circularly polarized light ( $E_{in} = [1 \ i]^T$ ). We set the wavelength at 1550 nm to characterize the properties of generated OAM-carrying vector beams. The employed metasurfaces has an orientation angle of  $\alpha(\varphi) = l\varphi + \alpha_0$ , where  $l$  varies from +3 to -3 and  $\alpha_0 = 0$ . We use  $E_1$  and  $E_2$  to represent the electric field components along directions of  $e_1(\varphi)$  and  $e_2(\varphi)$  in **Figure 5(b)**, respectively. The first row in **Figure 6** shows spatial phase distribution of  $E_1$ , indicating that output beams carry OAM with a charge number of  $l$  from +3 to -3. The second and third rows in **Figure 6** show spatial power distributions ( $P_1 \propto |E_1|^2$ ,  $P_2 \propto |E_2|^2$ ) along directions of  $e_1(\varphi)$  and  $e_2(\varphi)$ , respectively. It is found that the power component  $P_1$  is much larger than  $P_2$ . The extinction ratio (ER), defined by  $10 \times \log_{10}(P_1/P_2)$ , exceeds 20 dB. Hence, the electric field component  $E_2$  along the direction of  $e_2(\varphi)$  can be ignored. The fourth and fifth rows in **Figure 6** show spatial power distributions ( $P_x$ ,  $P_y$ ) along  $x$  and  $y$  axes, respectively. The alternative bright and dark power distribution implies that the polarization state rotates with the azimuthal angle  $\varphi$ . Distributions of spatial polarization are shown in **Figure 6** (sixth row),

indicating the vector beams producing with a polarization order of  $l$  changing from +3 to -3. Generation of vector beams carrying OAM utilizing the proposed metal metasurfaces is successfully confirmed in the simulated results.

The operation bandwidth is also studied. We considered the rectangular apertures in the metal film with orientation angle expression of  $\alpha(\varphi) = l\varphi + \alpha_0$  ( $l = 1, 2, 3$ ). We choose input optical beam

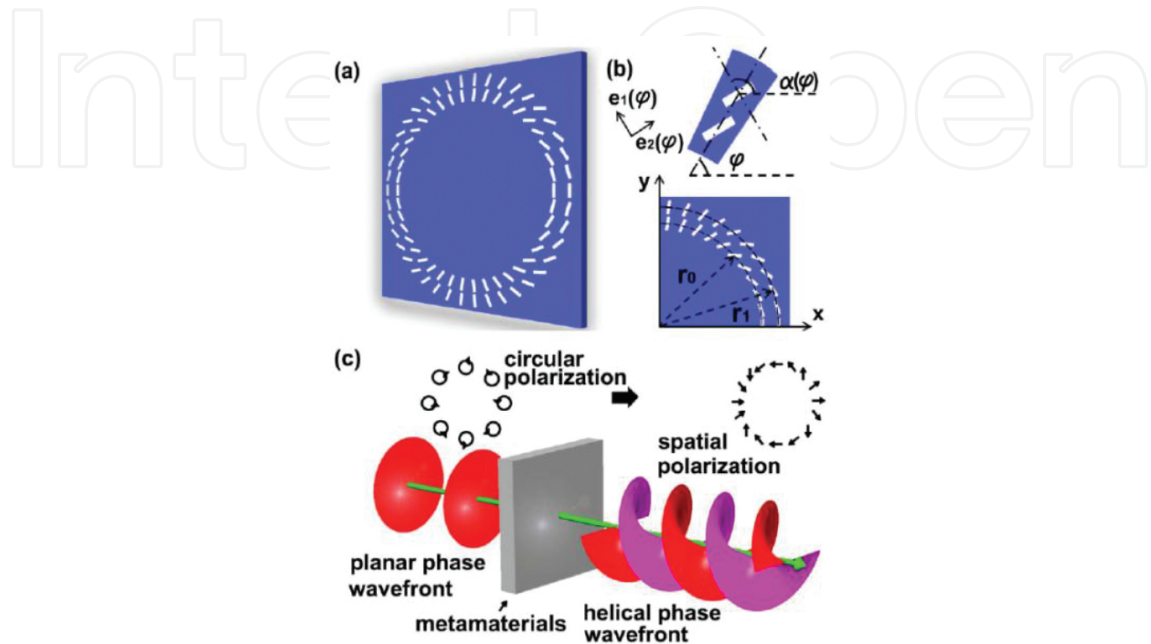


**Figure 5.** (a) Schematic diagram of metasurfaces for generating vector beams carrying OAM. (b) The radii of two concentric rings are  $r_i = (i+6.3) \times 700$  nm ( $i = 0, 1$ ) and the orientation angle respect to the  $x$  axis is  $\alpha(\varphi) = l\varphi + \alpha_0$  (e.g.,  $l = 2, \alpha_0 = 0$ ). The dimension of rectangular aperture is  $600 \times 140$  nm. (c) Concept of generating vector beam carrying OAM (OAM charge number is 2; polarization order is 2) [47].

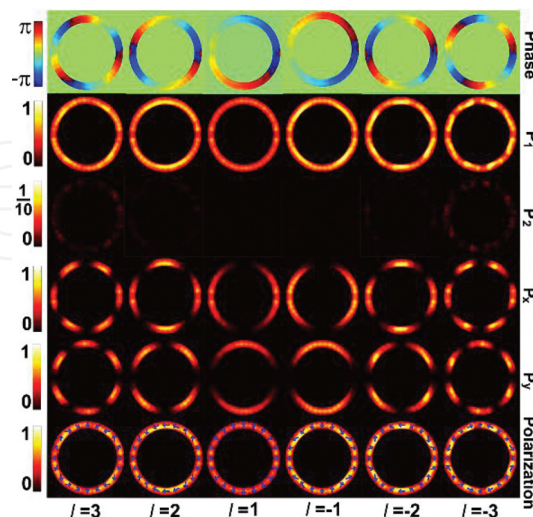


**Figure 6.** Spatial distributions of phase, power and polarization of generated OAM-carrying vector beams ( $\sigma = 1$ : left circularly polarized input beam,  $\alpha_0 = 0$ : along the direction of  $e_1(\varphi)$ ) [47].

of left circular polarization light as the stimulating source. ER and purity are used to analyze the quality of produced vector beams carrying OAM. **Figure 7(a)** shows the relationship between ER and wavelength. One can see that the produced vector beams carrying OAM have high quality in broadband regime of wavelength from 1000 to 2500 nm, covering parts of near-infrared band and mid-infrared band. For topological charge number  $l$  of 1 and 2, the ER is maintained above 20 dB covering the wavelength of 1000–2500 nm. For topological charge number  $l$  of 3, we achieve  $ER > 16$  dB covering the wavelength of 1000–2500 nm and  $ER > 20$  dB covering the wavelength of 1000–1800 nm. The purity as a function of wavelength of vector beam carrying OAM of  $l = 3$  is plotted in **Figure 7(b)**, achieving values above 0.85 covering the wavelength of 1000–2500 nm. The inset pictures show the relationship between weight spectra and topological charge numbers of OAM and polarization order at 1550 nm. The results show that we achieve high-values purities.

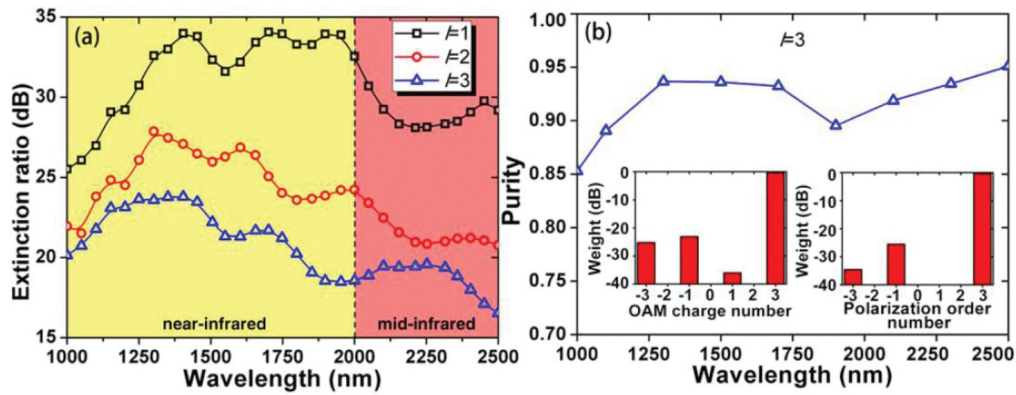


**Figure 7.** Wavelength-dependent (a) extinction ratio (ER) and (b) purity for the generation of OAM-carrying vector beams. Insets in (b) show weight as functions of OAM charge number (left) and polarization order number (right) at 1550 nm [47].

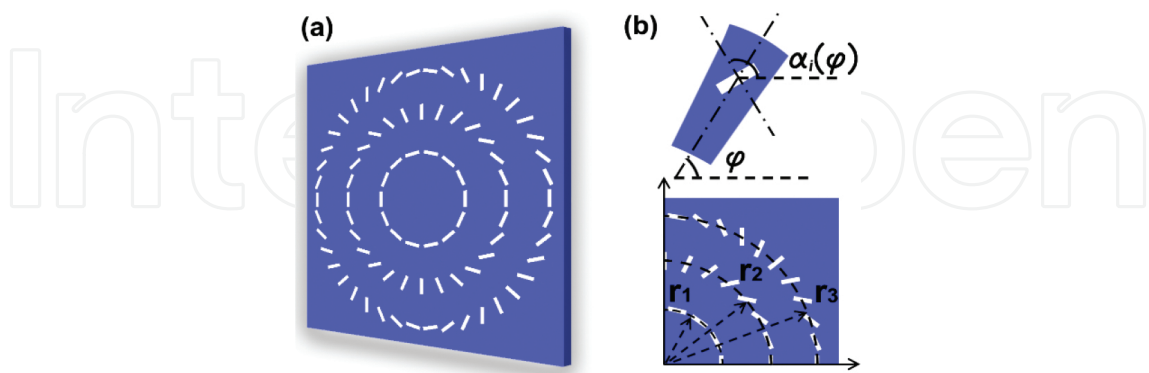


**Figure 8.** (a) Schematic diagram of proposed metasurfaces. (b) Details of rectangular aperture in the metasurface [48].

In **Figure 5(a)**, two concentric rings are used to excite a single OAM-carrying vector beam. Actually, one ring can also enable the generation of one OAM-carrying vector beam. Hence, it is possible to generate multiple OAM-carrying vector beams by forming multiple concentric

rings in a gold film as shown in **Figure 8**, where each ring contains a rectangular aperture array with each aperture acting as a localized polarizer. In particular, it is expected to selectively generate different orders of OAM-carrying vector beams by shining the circularly polarized light source onto different concentric rings.

**Figure 9(a)** shows ER as a function of wavelength. One can see broadband operation from 1000 to 1550 nm with an extinction ratio above 20 dB, which indicates high-quality broadband ( $\sim 500$  nm) generation of OAM-carrying vector beams. The fabrication tolerance of the proposed metasurface is also studied by analyzing the relationship between characteristic dependence and the initial orientation angle  $\alpha_{i0}$  of each rectangular aperture. The relationship between the extinction ratio and the initial orientation angle  $\alpha_{20}$  of each rectangular aperture in the metal film of the second ring is shown in **Figure 9(b)**. When the value of  $\alpha_{20}$  is changed from  $-1$  to  $7$  degrees, the extinction ratio is maintained over 20 dB. The initial orientation angle range is obtained near 8 degrees, indicating a favorable fabrication tolerance of the proposed metasurfaces. We use  $E_{1i}$  and  $E_{2i}$  to denote the electric field components on the directions of  $e_{1i}(\varphi)$  and  $e_{2i}(\varphi)$  (similar to  $e_1(\varphi)$  and  $e_2(\varphi)$  in **Figure 5(b)**), respectively. We calculate the phase of  $E_{1i}$  and the power components on directions of  $e_{1i}(\varphi)$ ,  $e_{2i}(\varphi)$ ,  $x$  and  $y$  axes, which are presented by  $P_{1r}$ ,  $P_{2r}$ ,  $P_{xr}$  and  $P_{yr}$ , respectively. We also calculated the state of spatially variant polarization of the vector beams carrying OAM. All these simulated results are displayed in **Figure 9(c)**. One can clearly indicate that the components of power on the direction of  $e_{1i}(\varphi)$  has a larger value than that of  $e_{2i}(\varphi)$ . In **Figure 9(c)**, the phase distributions indicate that the component of electric field  $E_{1i}$  has OAM with a topological charge number of  $m = i$  ( $i = 1, 2, 3$ ). Spatial distribution of  $P_{xr}$ ,  $P_{yr}$  and the polarization state confirm that the vector beams carrying OAM have a number of polarization order of  $l = i$  ( $i = 1, 2, 3$ ) can be confirmed by the spatial distributions of the polarization and power.

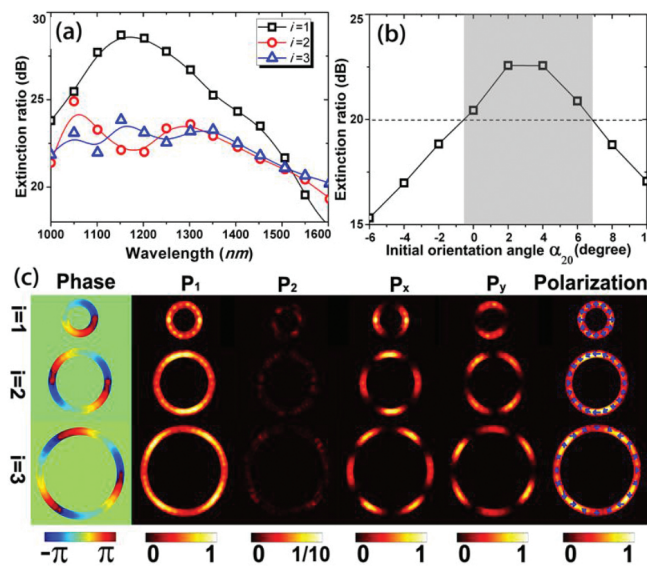


**Figure 9.** (a) Wavelength-dependent extinction ratio for three OAM-carrying vector beams. (b) The dependence of extinction ratio on the initial orientation angle  $\alpha_{20}$  (second ring). (c) Spatial distributions of phase, power components and polarization [48].

## 2.2. N-fold OAM multicasting using V-shaped antenna array [49]

We design a V-shaped antenna array to realize on-chip multicasting from a single Gaussian beam to four OAM beams. The concept and schematic diagram of N-fold optical multicasting of beams carrying OAM utilizing V-shaped antennas is displayed in **Figure 10**. At the side of multiple OAM multicasting, a specially designed V-shaped antenna array can be seen as a complex phase pattern that can manipulate the wavefront of the input Gaussian beam and then produce multiple OAM beams of collinearly superimposed propagation direction. Then the V-shaped antenna array can duplicate the messages carried by the input Gaussian beam and deliver to multiple optical beams carrying OAM of different topological charge number. Due to the phase singularity of optical beams carrying OAM, the intensity of superimposed multiple optical beams carrying OAM has a dark center. At the side of optical beams carrying OAM demultiplexing, the superimposed multiple optical beams carrying OAM are respectively distributed to multiple end users. At the side of each end user, the helical phase front of the desired optical beam carrying OAM is removed using an inverse phase pattern, resulting in a bright center in the intensity distribution, which can be conveniently separated from other optical beams carrying OAM using spatial filtering.

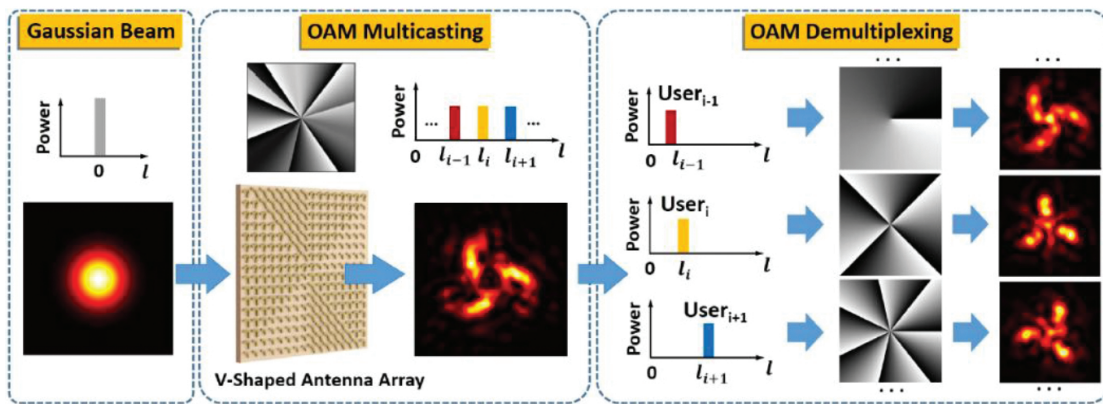


**Figure 10.** Concept and principle of N-fold multicasting of OAM beams using V-shaped antenna phase array [49].

To enable on-chip OAM multicasting, a pattern search assisted iterative (PSI) algorithm is employed to prepare a specific phase pattern for the simultaneous generation of multiple collinearly superimposed OAM beams. **Figure 11(a)** displays the calculated phase pattern using PSI algorithm to generate four collinearly superimposed OAM beams with charge values of  $l = 1, 4, 7, 10$ , respectively. Considering discrete unit of V-shaped antenna array, replace the simulated continuous complex phase pattern with a discrete one is necessary. The right picture of **Figure 11(a)** displays the simulated discrete phase pattern that discretizes the previous continuous complex phase pattern into 32 different values along the azimuthal direction. We then evaluate the degradation of performance of produced collinearly superimposed optical beams carrying OAM caused by the simulated discrete phase pattern by calculating and comparing power distributions of channels of optical beams carrying OAM produced by both continuous and discrete complex phase patterns, as depicted in **Figure 11(b)**. Here the crosstalk for all channels of optical beams carrying OAM is defined

by the power ratio of the desired channel of OAM beam (e.g.  $l = 4$ ) to its neighboring ones (e.g.  $l = 3$  and  $l = 5$ ). The crosstalk degradation of less than 2 dB is obtained for all four channels of OAM beam after passing through the discrete complex phase pattern. Then we design and simulate the V-shaped antenna array to achieve multicasting from a Gaussian beam to four optical beams carrying OAM by replacing the designed discrete complex phase pattern with corresponding V-shaped antennas, as plotted in **Figure 11(c)–(d)**.

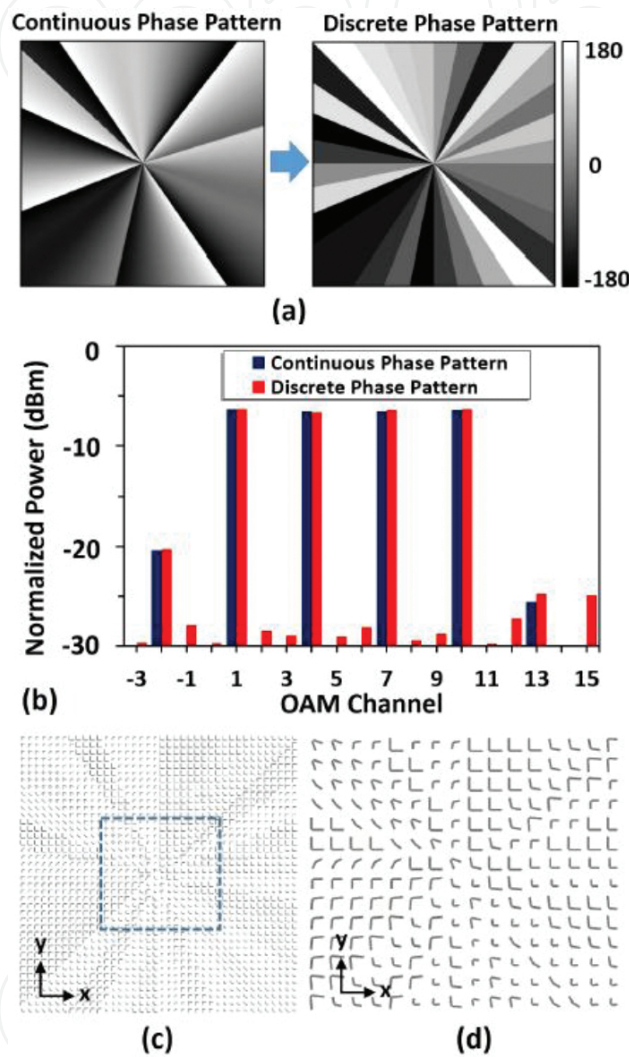


**Figure 11.** (a) Simulated continuous and discrete phase patterns. (b) Power distributions of channels with different topological charge number of OAM produced by continuous discrete phase patterns. (c) and (d) Top view of designed metal V-shaped antenna array to generate multicasting of optical beams carrying OAM [49].

The simulated intensity distribution of the multicasting optical beams carrying OAM produced by the designed V-shaped antenna array has a dark center, as plotted in **Figure 12(a)**. **Figure 12(b)** and (c) show the intensity distributions of channels of optical beams carrying OAM after demultiplexed by the inverse phase pattern. One can see that multicasting channels have bright spots in the center of the beams (**Figure 12(c)**), while undesired channels have dark centers in the intensity distributions (**Figure 12(b)**). We also simulate the power distribution

of channels with different topological charge number produced by the designed V-shaped antenna array, as displayed in **Figure 12(d)**. The cross talks of less than  $-15$  dB for all multicast channels are obtained, as plotted in **Figure 12(d)**.

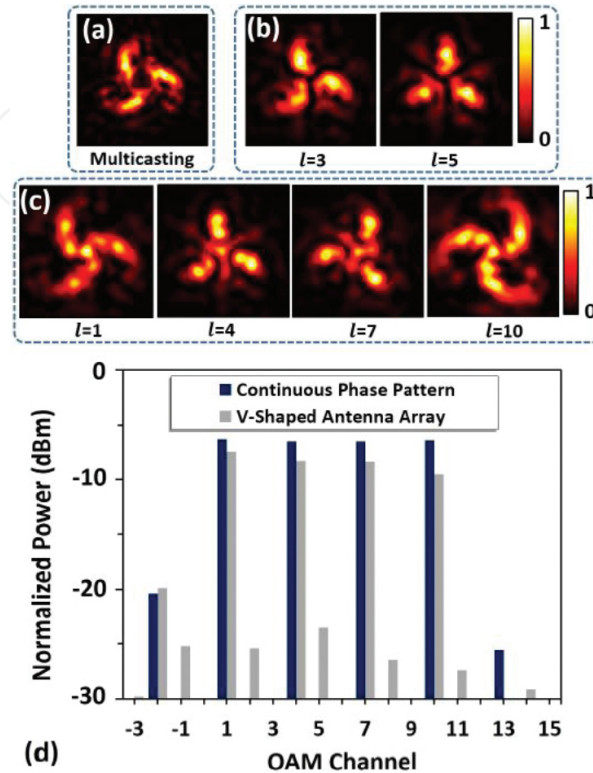


**Figure 12.** (a) Simulated intensity profiles of produced multicast four optical beams carrying OAM. (b) Simulated intensity profiles of undesired channels after demultiplexed by inverse phase pattern. (c) Simulated intensity profiles of multicasting channels after demultiplexed by inverse phase pattern. (d) Power distributions of channels with different topological charge number of OAM produced by designed V-shaped antenna array compared with that of continuous phase pattern [49].

### 2.3. Metasurface on conventional optical fiber facet for linearly polarized mode ( $LP_{11}$ ) generation

We design and fabricate metasurface on the facet of conventional G.652 single mode fiber (SMF) [50]. Here we choose metal rectangle resonator as a unit structure of metasurface. The working principle of a metal rectangle resonator can be explained as follows: the polarization of incident light is along  $x$  polarized, which can be decomposed into two perpendicular components corresponding to the long and short edge of the resonator, respectively; the transmission amplitudes of response for a resonator in both components are almost the same while the relative phase retardation is around  $\pi$ , where the linear polarization conversion occurs, resulting in a  $y$ -polarized transmitted light. Finite-difference time-domain (FDTD) method is also used to simulate the amplitude and phase response of proposed metal rectangle resonator and its mirror image. The amplitude responses of  $y$ -polarized transmitted light of this resonator and its mirror image are almost the same while the phase

responses of them have a difference of  $\pi$ . Therefore, this feature can be used to generate higher-order LP mode in the optical fiber. When an  $x$  polarized Gaussian beam is irradiating on the metasurface on the facet of G.652 SMF at wavelength of 632.8 nm, it can generate two kinds of transmitted beams with orthogonal polarization. Transmitted beam with  $x$  polarization called normal refractive beam that is not influenced by the metasurface can generate LP<sub>01</sub> mode. Meanwhile, transmitted beam with  $y$  polarization called abnormal refractive beam that is influenced by the metasurface can generate LP<sub>11</sub> mode. Owing to the orthogonal polarization of generated LP<sub>01</sub> and LP<sub>11</sub> modes, it is significantly convenient to separate these two modes in optical fiber. **Figure 13(a)** and **(b)** shows the fabricated metasurface on the facet of G.652 SMF to generate LP<sub>11</sub> mode. The experimental results can be seen in **Figure 13(d)–(g)**. When the polarization direction of incident light is set along  $x$ -axis, the LP<sub>01</sub> mode is  $x$ -polarized and LP<sub>11</sub> mode is  $y$ -polarized, as plotted in **Figure 13(d)** and **(e)**. When the polarization direction of incident light is changed to  $y$ -axis, the polarization directions of LP<sub>01</sub> and LP<sub>11</sub> mode exchange, as seen in **Figure 13(f)** and **(g)**.

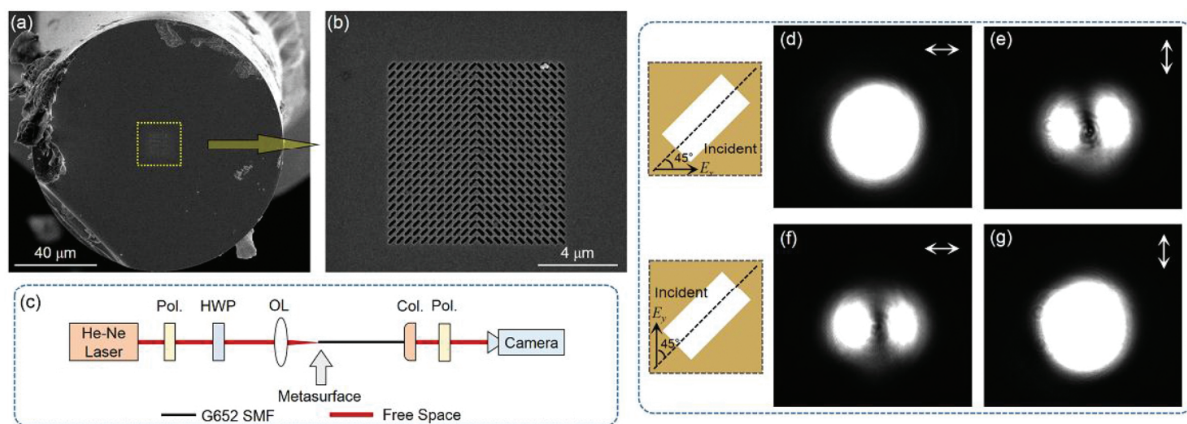


**Figure 13.** (a) and (b) SEM images of top view of a fabricated metasurface on the facet of SMF to generate LP<sub>11</sub> mode: (b) details of the metasurface array. (c) Experimental setup for LP<sub>11</sub> mode generation using the fabricated metasurface. Pol.: polarizer; HWP: half-wave plate; OL: objective lens; Col.: collimator. (d)–(g) Measured intensity profiles of generated LP<sub>11</sub> mode and LP<sub>01</sub> mode using the fabricated metasurface on the facet of SMF [50].

### 3. Light manipulation using dielectric metasurfaces

Dielectric metasurfaces are composed of high refractive index dielectric nanoparticles based on the Mie resonances. Several typical types of dielectric metasurfaces and previous relevant researches have been reported: (1) Er-doped Si-rich silicon nitride nanopillar array is designed and fabricated using RF magnetron sputtering, electron beam lithography, and reactive ion etching methods for enhanced omnidirectional light extraction and OAM beams generation [34]; (2) Si-based metasurfaces are designed and fabricated using electron-beam lithography and reactive ion etching techniques to possess sharp electromagnetically induced–transparency-like resonances in the near-infrared regime [41]; (3) silicon nanobeams antennas are designed and fabricated using low-pressure chemical vapor deposition (LPCVD), electron-

beam lithography, and reactive ion etching techniques to generate Bessel beams [29]; (4) amorphous-silicon nanoridges are designed and fabricated using standard electron-beam lithography, and reactive ion etching techniques to realize polarization beam splitting in pixel-level [36]; (5) silicon nanodisks are designed and fabricated using chemical vapor deposition, electron-beam lithography, and reactive ion etching methods to achieve high transmission and full-phase control in visible wavelength [53]; (6) silicon cut-wires array in combination with a silver ground plane are designed and fabricated using chemical vapor deposition, electron-beam lithography, and reactive ion etching techniques to achieve high linear polarization conversion efficiency in the near-infrared band [54]; (7) silicon nanopillar array is designed and fabricated using electron-beam lithography and reactive ion etching techniques to realize low loss micro-lenses in the near-infrared band [55]; (8) dielectric metasurface with a tailored-phase gradient is designed to achieve carpet cloaking at microwave frequencies [56]. All these previous works are based on manipulating the Mie responses of dielectric nanoparticles by altering the dimensions, directions, arrangement of unit structures and even combining multiple resonators with different shapes. Recently, we have also made some progresses in dielectric metasurfaces on the basis of previous works.

### 3.1. OAM beams generation using nanophotonic dielectric metasurface array

We design and fabricate a kind of chip-scale dielectric metasurface array on silicon-on-insulator (SOI) platform. **Figure 14** shows the schematic drawing of the proposed dielectric metasurface units, consisting of rectangle or ellipse silicon resonators with various dimensions. The working principle of these proposed dielectric resonators can be explained as follows: the polarization of incident light is along  $x$ -axis, which can be decomposed into two perpendicular components corresponding to the long and short axis of the resonator, respectively; the reflection amplitudes of response for a resonator in both components are almost the same while the relative phase retardation is around  $\pi$ , where the linear polarization conversion occurs, resulting in a  $y$ -polarized reflected light [51].

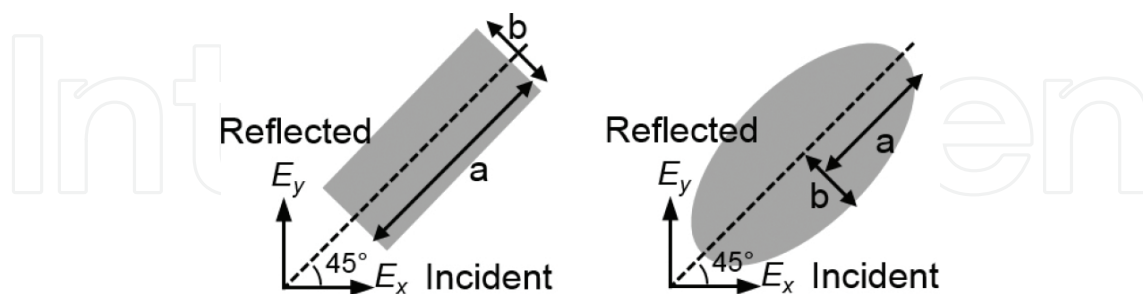


**Figure 14.** Schematic diagram of top view of designed reflective dielectric rectangle/ellipse metasurface units based on silicon-on-insulator (SOI) platform.

Then we simulate the amplitude and phase responses of the near-field of reflected light of a rectangle dielectric metasurface unit with various dimensions using FDTD method at the wavelength of 1064 nm. The simulated results indicate that the response of the proposed resonator can cover a full phase varying over  $0-2\pi$  and wide shift of amplitude. It is relatively

easy to find out a series of resonators covering full-phase control while maintaining approximately constant amplitude, which is considerably important for OAM beams generation. Then eight kinds of resonators with different geometric dimensions are chosen to provide an equal-spacing phase shift from 0 to  $2\pi$  and nearly constant amplitude, as plotted in **Figure 15**. **Figure 16** plots the simulated intensity and phase distributions of OAM beams of topological charge number  $l = 1-4$  generated using the rectangle dielectric metasurface array consisted of the eight chosen resonators. The results indicate that the generated OAM beams match the theoretical ones well.

Moreover, we also design the dielectric ellipse metasurface arrays at the wavelength of 632.8nm. **Figure 17** shows the concept of OAM beams generation through dielectric ellipse

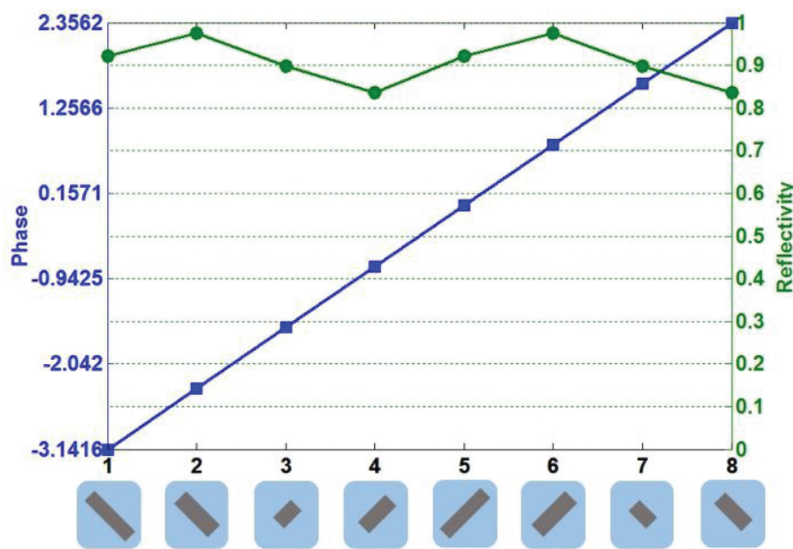


**Figure 15.** Schematic of eight dielectric rectangle resonators chosen to generate OAM beams, providing a phase shift from 0 to  $2\pi$  and nearly constant amplitude.

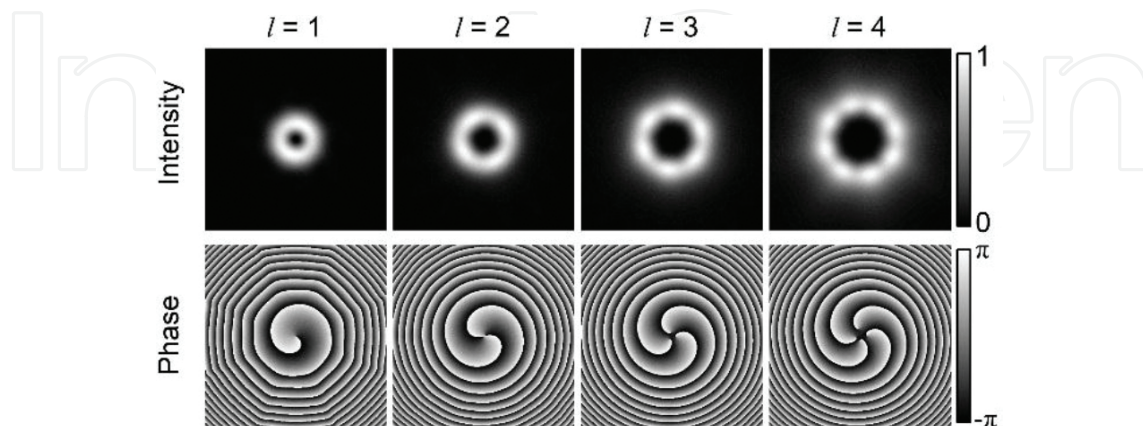


**Figure 16.** Simulated intensity and phase distributions of generated OAM beams by proposed rectangle dielectric metasurface array at the wavelength of 1064 nm.

metasurface array consisting of a series of resonators covering a full-phase modulation. When a Gaussian beam of vertical polarization is incident to the metasurface, the reflected beam can be transformed into OAM beams of horizontal polarization. In view of polarization conversion happened on the proposed metasurface, one can easily separate the incident and reflected lights. **Figure 18** plots the simulated intensity and phase distributions of OAM beams of topological charge number  $l = -4$  to 4 generated using the dielectric ellipse metasurface array consisted of the eight chosen resonators at the wavelength of 632.8 nm. The results indicate that the generated OAM beams match the theoretical ones well.

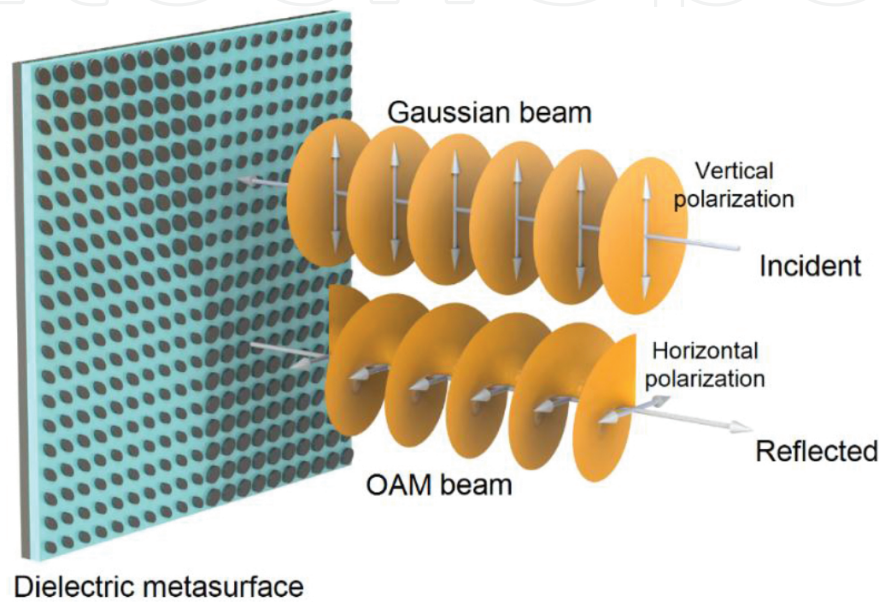


**Figure 17.** Concept of OAM beams generation using dielectric ellipse metasurface array.

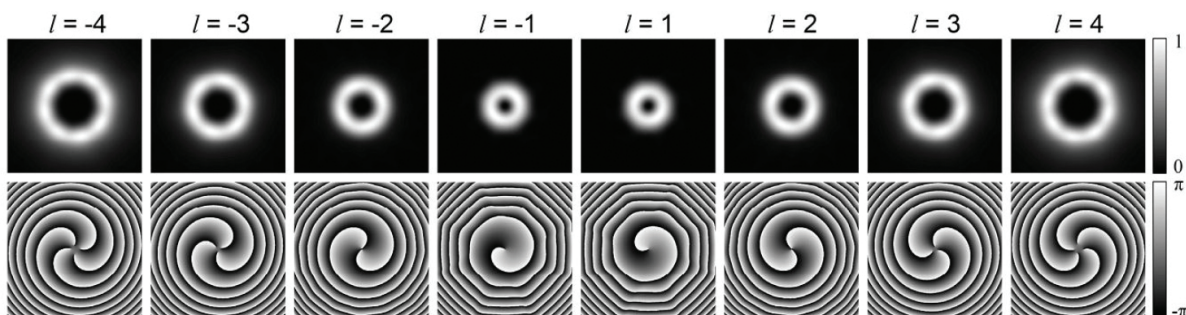


**Figure 18.** Simulated intensity and phase distributions of generated OAM beams by proposed dielectric ellipse metasurface array at the wavelength of 632.8 nm [51].

We further fabricate and test the designed dielectric ellipse metasurface arrays at the wavelength of 632.8 nm. **Figure 19** shows the experimental results of fabricated dielectric ellipse metasurface arrays. The first line in **Figure 19** plots the measured intensity profiles of generated OAM beams of  $l = -4$  to 4 using the fabricated metasurface arrays. The second line in **Figure 19**

exhibits the measured intensity profiles of generated OAM beams after interfered by Gaussian beam. One can clearly see from **Figure 19** that the number of the helical arms in the distribution of interference intensity is equal to the topological number  $l$  of OAM beam, indicating the favorable results.

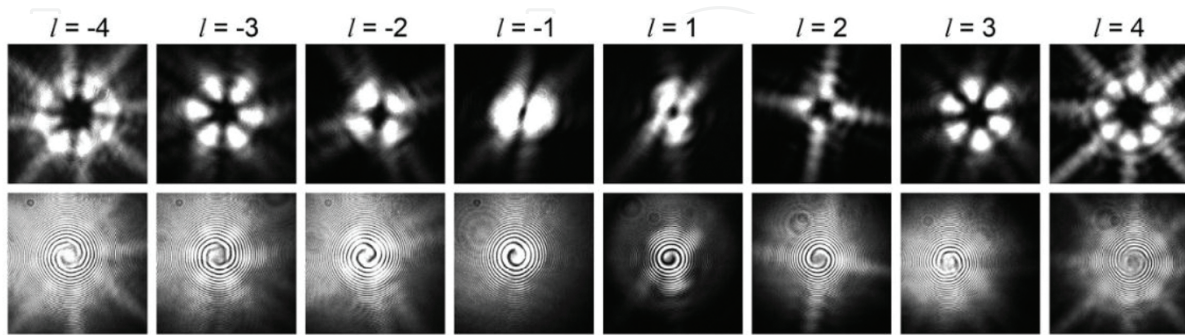


**Figure 19.** Experimental intensities of generated OAM beams of  $l = -4$  to 4 by proposed dielectric metasurface array at the wavelength of 632.8 nm (first line). Experimental intensities of generated OAM beams after interfered by Gaussian beam with  $l = 0$  (second line) [51].

### 3.2. Bessel beams generation and OAM multicasting using dielectric metasurface array

We propose and design dielectric ellipse metasurfaces to realize Bessel beams generation and OAM multicasting at the wavelength of 1550 nm, as displayed in **Figure 20(a)** [52]. **Figure 20(b)** and **(c)** respectively depict the simulated amplitude and phase responses of  $y$ -polarized reflected light using FDTD method. Then we choose eight kinds of resonators with different geometric dimensions as shown in **Figure 21(a)**, providing a phase shift from 0 to  $2\pi$  and nearly constant amplitude. The method of phase pattern replacing axicon is used to generate Bessel beams. By replacing the phase patterns with the eight chosen resonators, simulated Bessel beams are achieved as plotted in **Figure 21(b)**. The purities of generated Bessel beams with different indices are also analyzed. As shown in **Figure 21(c)**, the purities of generated Bessel beams with different indices of  $l = -20, -19, \dots, 19, 20$  are all higher than 0.93.

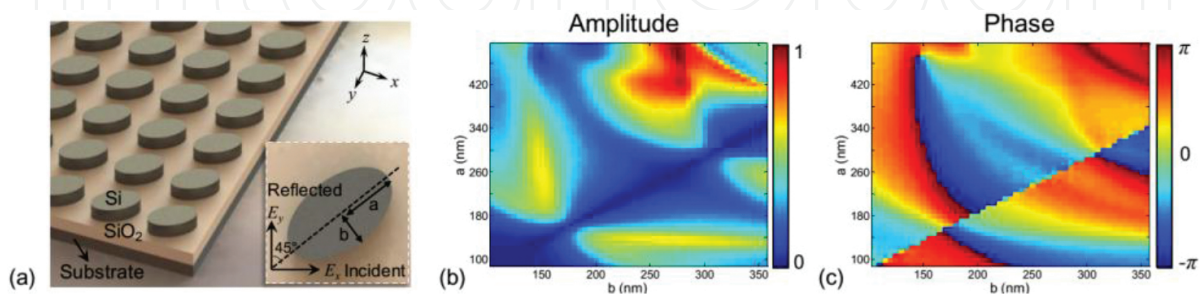


**Figure 20.** (a) Schematic diagram of designed dielectric ellipse metasurface with a period of 1  $\mu\text{m}$  and silicon height of 500 nm. Inset is the top view of a dielectric elliptical resonator. (b) and (c) are simulated near-field amplitude and phase of  $y$ -polarized reflected light as functions of half of long axis length  $a$  and short axis length  $b$  [52].

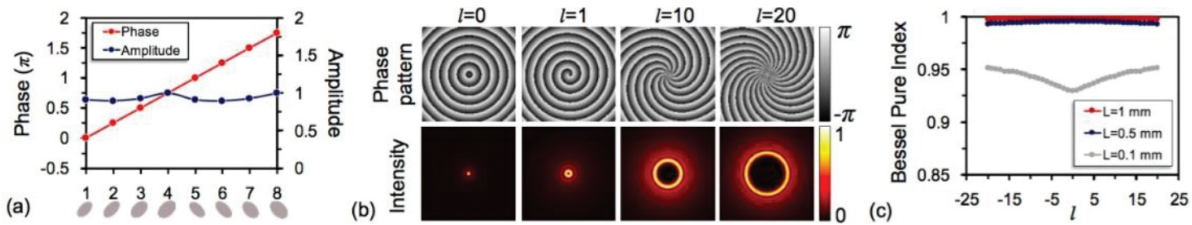


**Figure 21.** (a) Schematic of eight resonators chosen to generate Bessel beams, providing a phase shift from 0 to  $2\pi$  and nearly constant amplitude. (b) Simulated intensity of four Bessel beams ( $l = 0, 1, 10, 20$ ) by replacing the corresponding phase patterns with the eight chosen resonators. (c) Purities of generated Bessel beams with different indices versus topological number  $l$  with varied propagation length  $L$  [52].

Moreover, sixfold OAM multicasting using the designed dielectric ellipse metasurfaces is also simulated. The ideal phase pattern to generate collinearly superimposed six OAM beams ( $l = 1, 4, 7, 10, 13, 16$ ) is plotted in **Figure 22(a)**. By replacing the ideal phase pattern with corresponding resonators, we design the dielectric ellipse array shown in **Figure 22(b)**. The intensity profile of the superimposed six OAM modes produced by the proposed ellipse array with a trigonal dark center is depicted in **Figure 22(d)**. **Figure 22(e)** and **(f)** shows the intensity profiles of OAM channels after demultiplexing. For desired OAM channels, a bright light spot emerges at the center of beam (**Figure 22(f)**), while for needless channels, dark region will come out at the beam center (**Figure 22(e)**). The power ratios of the needed OAM channels (e.g.  $l = 16$ ) to its neighboring ones (e.g.  $l = 15$  and  $l = 17$ ) are defined as cross talks, which are approximately less than  $-14$  dB as plotted in **Figure 22(c)**.

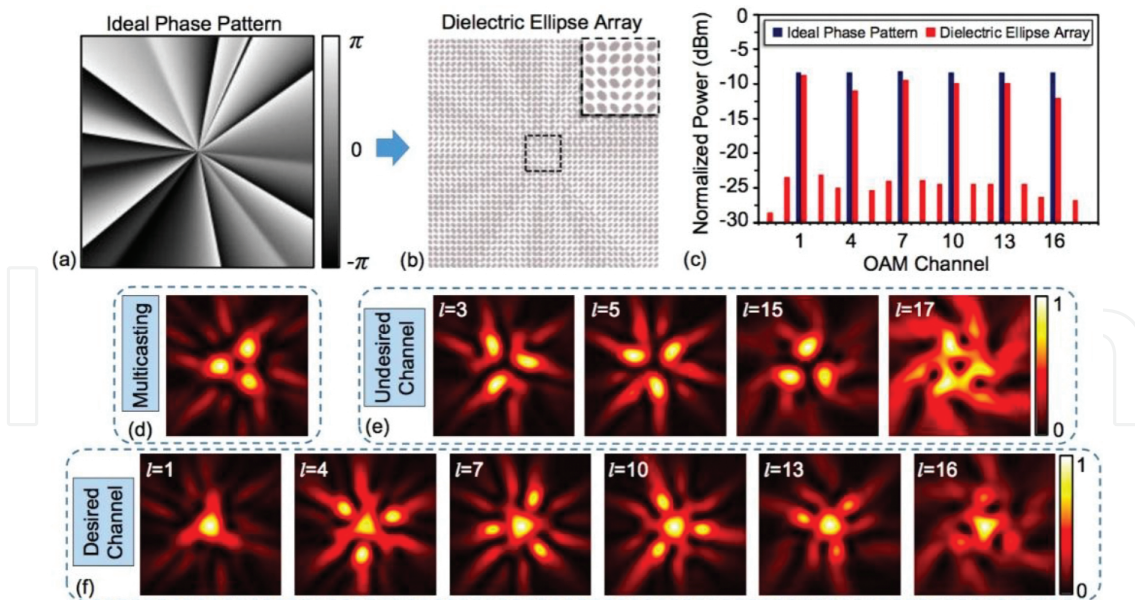


**Figure 22.** (a) Ideal phase pattern to generate sixfold OAM multicasting ( $l = 1, 4, 7, 10, 13, 16$ ). (b) Top view of designed dielectric ellipse array to generate sixfold OAM multicasting by replacing the ideal phase pattern with corresponding resonators. (c) Power distributions of OAM channels generated by ideal phase pattern and dielectric ellipse array. (d) Intensity distribution of collinearly superimposed six OAM beams. (e) Intensity distribution of undesired OAM channels after demultiplexing. (f) Intensity distribution of multicasting OAM channels after demultiplexing [52].

## 4. Discussion

Although metasurfaces composed of plasmonic and dielectric units have only recently emerged as an active area of research, their potential as an approach to realize light manipulation devices has already been successfully implemented in flat optics such as OAM beams generator, lens, wave plates, holograms, and so on, for its superiorities of compact and flexible design. For instance, convenient optical elements are based on refraction, reflection or diffraction of light. Their ability of wavefront shaping is relay on propagation through media whose refractive indices can be designed to control the light path. As a consequence, those conventional optical elements suffer from thick materials, large volume, long diffraction distance and even low optical manipulation accuracy that they are difficult to be compatible with compact systems. Metasurface-based flat optical elements can potentially replace traditional ones. They are able to modulate wavefront of light beam by introducing a variety of nanoscaled electric dipole resonators replacing conventional propagation effect and therefore considerably reduce the whole volume of systems. Besides, the responses of metasurfaces rely on the characteristics of unit structures such as structure dimensions and materials types. It is relatively convenient to flexibly control the amplitude, phase and polarization of scattering light.

However, there are still some challenges of metasurfaces. For plasmonic metasurfaces, they suffer from ohmic loss at optical wavelength. One common solution to loss compensation is to introduce a gain medium in or around the plasmonic material. This solution can partially or fully compensate the loss in metals, but the incorporation of such active materials is very challenging [57]. Another challenge for plasmonic metasurfaces is that noble metals have large plasma frequency and cannot be adjusted, making tunable or switchable metasurface devices hard to realize [57]. What is more, noble metals are not compatible with the standard semiconductor fabrication technologies, restricting metasurface devices to the proof-of-concept stage only. To deal with those issues, some recent researches focus on new materials platforms defined new, intermediate carrier density materials as the best candidates that perform low loss, excellent tuning, and modulation capabilities and that are compatible with established semiconductor processing technologies and integration procedures [57, 58]. In addition, metasurfaces are also facing the challenge of reconfigurable. For metasurface, the unit structures must be subwavelength-scaled optical switches with a fraction of a square micrometer footprint and a volume of only approximate  $10^{-19}$  m<sup>3</sup>. The optical switches are desired to be fast and energy saving. It is challenging for unit structures to satisfy the former two conditions. To solve the problem, one can alter the dimensions of individual unit structures, or manipulate the near-field interactions between them. The nanomechanical devices platform can provide one possible ideal solution. There are several impressive works reported recently focusing on the tunable and reconfigurable metasurfaces [57, 58]: (1) by combining the Fano resonant metal nanoparticles with a single layer graphene, obviously electrically controlled damping are observed in the Fano resonances in the near-infrared regime; (2) by positioning a thin graphene sheet over asymmetric silicon nanobars, transmission spectrum of the proposed device can be efficiently adjusted at the near-infrared frequencies; (3) a metal nanomechanical metasurface is fabricated on the nanoscale-thickness dielectric membrane,

and the displacement of metamolecules can be controlled by light illumination; (4) using differential thermal expansion and Lorentz force, electrothermal tuning and magnetic modulation are achieved in a reconfigurable metal metasurface; (5) using a vanadium dioxide metasurface lens, the amplitude spectrum and the focal intensity can be adjusted by changing the temperature in the terahertz regime; (6) utilizing a heating-induced vanadium dioxide planar metamaterial, the device is able to be switched between capacitive and inductive responses; (7) by combing metal nanoantenna array with indium tin oxide, phase and amplitude of reflected light can be controlled at near infrared wavelengths.

In spite of facing many challenges, metasurfaces are still one of the most potential devices applied in beam-steering, spatial light modulator, nanoscale-resolution imaging, sensing, and novel quantum optics devices. Besides, the increasing demand for large capacity of data transmission and fast signal processing promotes to eliminate the bottleneck between optical fiber communication networks and electronic data handling. Achieving this goal will require strong and fast nonlinearities for switching light with light, and much improved manipulation of the electromagnetic fields with external stimuli such as electric signals in compact space. Metasurfaces-based devices can considerably enhance these functionalities by exploiting the characteristics of metasurfaces [58]. In the future, metasurfaces-based devices would be in developing tunable, reconfigurable, nonlinear, switchable, gain and quantum metasurfaces, which might be achieved by adopting new materials (such as superconductors or graphene) and hybridizing plasmonics metal nanostructures with other functional materials such as nanocarbon, organics, nanosemiconductors, organic polymers and phase-change media [58].

## 5. Conclusion

In summary, we have reviewed our recent works in light manipulation on the dimension of spatial structure using metasurfaces: (1) metasurfaces consisting of multiple concentric rings in a gold film are designed to generate broadband OAM carrying vector beams in the regime from near infrared to mid infrared band; (2) a metal V-shaped antenna array is designed to realize multicasting from a single Gaussian beam to four OAM beams assisted by PSI algorithm, achieving a low-crosstalk of near  $-15$  dB; (3) a kind of gold metasurface is designed and fabricated on the facet of a G.652 SMF to generate  $LP_{11}$  mode at the wavelength of  $632.8$  nm; (4) a kind of dielectric metasurface is designed and fabricated on SOI platform, realizing OAM beams generation; (5) a kind of dielectric metasurface is designed on SOI platform at the wavelength of  $1550$  nm, achieving Bessel beams generation with high purity and multicasting from a single Gaussian beam to six OAM beams with a relatively low crosstalk less than  $-14$  dB. The designed and fabricated metasurfaces in these works have nanoscaled dimensions and the generated beams carrying OAM have favorable qualities, which are promising for compact and effective beam-steering system and space-division multiplexing (SDM)-assisted optical communication systems. In the future, the metasurface devices to generate optical beams carrying OAM can combine with tunable and reconfigurable functions reported in Refs. [57–58], which makes robust spatial light manipulation possible and facilitates more interesting applications.

## Acknowledgements

This work was supported by the National Natural Science Foundation of China (NSFC) under Grants 11574001, 11274131, and 61222502, the National Basic Research Program of China (973 Program) under Grant 2014CB340004, the National Program for Support of Top-Notch Young Professionals, and the Program for New Century Excellent Talents in University (NCET-11-0182). The authors would like to thank Zhe Zhao, Xiao Hu, Nan Zhou, Long Zhu, Shuhui Li, Jun Liu, Yifan Zhao, and Hongya Wang for technical supports and helpful suggestions.

## Author details

Jian Wang\* and Jing Du

\*Address all correspondence to: [jwang@hust.edu.cn](mailto:jwang@hust.edu.cn)

Wuhan National Laboratory for Optoelectronics, School of Optical and Electronic Information, Huazhong University of Science and Technology, Wuhan, Hubei, China

## References

- [1] M. Born, W. Emil, Principles of optics: electromagnetic theory of propagation, interference and diffraction of light. Cambridge university press, Cambridge, 2000.
- [2] C. A. Brackett, "Dense wavelength division multiplexing networks: Principles and applications." IEEE J. Sel. Areas Commun. 8, 948–964 (1990).
- [3] S. L. Jansen, I. Morita, T. C. Schenk, H. Tanaka, "Long-haul transmission of 16× 52.5 Gbits/s polarization-division-multiplexed OFDM enabled by MIMO processing." J. Opt. Networking, 7, 173–182 (2008).
- [4] S. Kawanishi, "Ultrahigh-speed optical time-division-multiplexed transmission technology based on optical signal processing: feature issue on fundamental challenges in ultrahigh-capacity optical fiber communication systems." IEEE J. Quantum Electron. 34, 2064–2079 (1998).
- [5] D. J. Richardson, J. M. Fini, L. E. Nelson, "Space-division multiplexing in optical fibres." Nat. Photon. 7, 354–362 (2013).
- [6] P. J. Winzer, R. J. Essiambre, "Advanced modulation formats for high-capacity optical transport networks." J. Lightw. Technol. 24, 4711–4728 (2006).
- [7] I. Moreno, J. A. Davis, B. M. L. Pascoguin, M. J. Mitry, D. M. Cottrell, "Vortex sensing diffraction gratings." Opt. Lett. 34, 2927–2929 (2009).

- [8] S. Bernet, A. Jesacher, S. Fürhapter, C. Maurer, M. Ritsch-Marte, "Quantitative imaging of complex samples by spiral phase contrast microscopy." *Opt. Express* 14, 3792–3805 (2006).
- [9] M. Padgett, R. Bowman, "Tweezers with a twist." *Nat. Photon.* 5, 343–348 (2011).
- [10] J. Leach, M. R. Dennis, J. Courtial, M. J. Padgett, "Laser beams: knotted threads of darkness." *Nature* 432, 165 (2004).
- [11] L. Paterson, M. P. MacDonald, J. Arlt, W. Sibbett, P. E. Bryant, K. Dholakia, "Controlled rotation of optically trapped microscopic particles." *Science* 292, 912–914 (2001).
- [12] D. R. Smith, W. J. Padilla, D. C. Vier, S. C. Nemat-Nasser, S. Schultz, "Composite medium with simultaneously negative permeability and permittivity." *Phys. Rev. Lett.* 84, 4184–4187 (2000).
- [13] W. Cai, V. Shalaev, *Optical Metamaterials: Fundamentals and Applications*. Springer Science and Business Media, New York, 2009.
- [14] N. Meinzer, W. L. Barnes, I. R. Hooper, "Plasmonic meta-atoms and metasurfaces." *Nature Photon.* 8, 889–898 (2014).
- [15] J. D. Jackson, *Classical Electrodynamics*. Wiley, New York, 1998.
- [16] V. M. Shalaev, W. S. Cai, U. K. Chettiar, H. K. Yuan, A. K. Sarychev, V. P. Drachev, A. V. Kildishev, "Negative index of refraction in optical metamaterials." *Opt. Lett.* 30, 3356–3358 (2005).
- [17] M. W. Klein, C. Enkrich, M. Wegener, S. Linden, "Second-harmonic generation from magnetic metamaterials." *Science* 313, 502–504 (2006).
- [18] S. Linden, C. Enkrich, M. Wegener, J. F. Zhou, T. Koschny, C. M. Soukoulis, "Magnetic response of metamaterials at 100 terahertz." *Science* 306, 1351–1353 (2004).
- [19] N. Fang, H. Lee, C. Sun, X. Zhang, "Sub-diffraction-limited optical imaging with a silver superlens." *Science* 308, 534–537 (2005).
- [20] E. Plum, V. A. Fedotov, A. S. Schwanecke, N. I. Zheludev, Y. Chen, "Giant optical gyrotropy due to electromagnetic coupling." *Appl. Phys. Lett.* 90, 223113 (2007).
- [21] J. B. Pendry, D. Schurig, D. R. Smith, "Controlling electromagnetic fields." *Science* 312, 1780–1782 (2006).
- [22] N. Yu, P. Genevet, M. A. Kats, F. Aieta, J. P. Tetienne, F. Capasso, Z. Gaburro, "Light propagation with phase discontinuities: generalized laws of reflection and refraction." *Science* 334, 333–337 (2011).
- [23] S. Jahani, Z. Jacob, "All-dielectric metamaterials." *Nat. Nanotech.* 11, 23–36 (2016).
- [24] C. F. Bohren, D. R. Huffman, *Absorption and Scattering of Light by Small Particles*. John Wiley & Sons, Hoboken, 2008.

- [25] M. Decker, I. Staude, M. Falkner, J. Dominguez, D. N. Neshev, I. Brener, T. Pertsch, Y. S. Kivshar, "High-efficiency dielectric Huygens' surfaces." *Adv. Opt. Mater.* 3, 813–820 (2015).
- [26] C. Enkrich, F. Perez-Williard, D. Gerthsen, J. Zhou, T. Koschny, C. M. Soukoulis, M. Wegener, S. Linden, "Focused-ion-beam nanofabrication of near-infrared magnetic metamaterials," *Adv. Mater.* 17, 2547 (2005).
- [27] S. R. J. Brueck, "Optical and interferometric lithography-nanotechnology enablers," *Proc. IEEE* 93, 1704 (2005).
- [28] S. Y. Chou, P. R. Krauss, P. J. Renstrom, "Nanoimprint lithography," *J. Vac. Sci. Technol. B* 14, 4129 (1996).
- [29] W. Wu, E. Kim, E. Ponizovskaya, Z. Liu, Z. Yu, N. Fang, Y. R. Shen, A. M. Bratkovsky, W. Tong, C. Sun, X. Zhang, S.-Y. Wang, R. S. Williams, "Optical metamaterials at near and mid-IR range fabricated by nanoimprint lithography," *Appl. Phys. A* 87, 147 (2007).
- [30] N. Yu, F. Aieta, P. Genevet, M. A. Kats, Z. Gaburro, F. Capasso, "A broadband, background-free quarter-wave plate based on plasmonic metasurfaces." *Nano Lett.* 12, 6328–6333 (2012).
- [31] S. Sun, K. Y. Yang, C. M. Wang, T. K. Juan, W. T. Chen, C. Y. Liao, Q. He, S. Xiao, W. T. Kung, G. Y. Guo, L. Zhou, D. P. Tsai, "High-efficiency broadband anomalous reflection by gradient meta-surfaces." *Nano Lett.* 12, 6223–6229 (2012).
- [32] S. Sun, Q. He, S. Xiao, Q. Xu, X. Li, L. Zhou, "Gradient-index meta-surfaces as a bridge linking propagating waves and surface waves." *Nat. Mater.* 11, 426–431 (2012).
- [33] F. Aieta, P. Genevet, M. A. Kats, N. Yu, R. Blanchard, Z. Gaburro, F. Capasso, "Aberration-free ultrathin flat lenses and axicons at telecom wavelengths based on plasmonic metasurfaces." *Nano Lett.* 12, 4932–4936 (2012).
- [34] D. Parker, D. C. Zimmermann, "Phased arrays—part 1: Theory and architectures." *IEEE Trans. Microwave Theory Tech.* 50, 678–687 (2002).
- [35] A. Pors, M. G. Nielsen, R. L. Eriksen, S. I. Bozhevolnyi, "Broadband focusing flat mirrors based on plasmonic gradient metasurfaces." *Nano Lett.* 13, 829–834 (2013).
- [36] J. J. Cowan, "The surface plasmon resonance effect in holography." *Opt. Comm.* 5, 69–72 (1972).
- [37] L. Huang, X. Chen, H. Mühlenbernd, H. Zhang, S. Chen, B. Bai, Q. Tan, G. Jin, K. W. Cheah, C. W. Qiu, J. Li, T. Zentgraf, J. Li, "Three-dimensional optical holography using a plasmonic metasurface." *Nat. Commun.* 4, 2808 (2013).
- [38] Z. H. Jiang, S. Yun, L. Lin, J. A. Bossard, D. H. Werner, T. S. Mayer, "Tailoring dispersion for broadband low-loss optical metamaterials using deep-subwavelength inclusions." *Sci. Rep.* 3, 1571 (2013).

- [39] M. Kang, J. Chen, X.-L. Wang, H.-T. Wang, "Twisted vector field from an inhomogeneous and anisotropic metamaterial." *J. Opt. Soc. Am. B* 29, 572–576 (2012).
- [40] L. Huang, X. Chen, H. Mühlhensbernd, G. Li, B. Bai, Q. Tan, G. Jin, T. Zentgraf, S. Zhang, "Dispersionless phase discontinuities for controlling light propagation." *Nano Lett.* 12, 5750–5755 (2012).
- [41] M. Khorasaninejad, W. Zhu, K. B. Crozier, "Efficient polarization beam splitter pixels based on a dielectric metasurface." *Optica* 2, 376–382 (2015).
- [42] N. Segal, S. Keren-Zur, N. Hendler, T. Ellenbogen, "Controlling light with metamaterial-based nonlinear photonic crystals." *Nat. Photon.* 9, 180–184 (2015).
- [43] S. Kim, H. Wakatsuchi, J. J. Rushton, D. F. Sievenpiper, "Switchable nonlinear metasurfaces for absorbing high power surface waves." *Appl. Phys. Lett.* 108, 041903 (2016).
- [44] X. Yin, Z. Ye, J. Rho, Y. Wang, X. Zhang, "Photonic spin Hall effect at metasurfaces." *Science* 339, 1405–1407 (2013).
- [45] Y. Yang, I. I. Kravchenko, D. P. Briggs, J. Valentine, "All-dielectric metasurface analogue of electromagnetically induced transparency." *Nat. Commun.* 5, 6753 (2014).
- [46] S. Mühlig, M. Farhat, C. Rockstuhl, F. Lederer, "Cloaking dielectric spherical objects by a shell of metallic nanoparticles." *Phys. Rev. B* 83, 195116 (2011).
- [47] Z. Zhao, J. Wang, S. Li, A. E. Willner, "Metamaterials-based broadband generation of orbital angular momentum carrying vector beams." *Opt. Lett.* 38, 932–934 (2013).
- [48] Z. Zhao, J. Wang, S. Li, A. E. Willner, "Selective Broadband Generation of Orbital Angular Momentum Carrying Vector Beams Using Metamaterials." *Proc. CLEO2013*, Optical Society of America, paper QM4A. 7, 2013.
- [49] J. Du, J. Wang, "Design of on-chip N-fold orbital angular momentum multicasting using V-shaped antenna array." *Sci. Rep.* 5, 9662 (2015).
- [50] J. Du, S. Chen, J. Liu, S. Li, L. Zhu, Y. F. Zhao, J. Wang, "Design and fabrication of metasurface on conventional optical fiber facet for linearly polarized mode (LP<sub>11</sub>) generation at visible light wavelength." *Proc. CLEO2016*, Optical Society of America (OSA), paper JTU5A.104, 2016.
- [51] J. Du, X. Li, S. Li, L. Zhu, N. Zhou, J. Liu, S. Chen, Y. Zhao, J. Wang, "Experimental demonstration of chip-scale orbital angular momentum (OAM) beams generation and detection using nanophotonic dielectric metasurface array." *Proc. OFC2016*, Optical Society of America (OSA), paper W2A.13, 2016.
- [52] J. Du, Z. Xu, L. Zhu, S. Li, J. Wang, "Design of On-Chip Dielectric Elliptical Meta-Reflectarray for Bessel Beams Generation and N-Fold Orbital Angular Momentum (OAM) Multicasting." *Proc. CLEO2015*, Optical Society of America (OSA), paper JTU5A.57, 2015.

- [53] Y. F. Yu, A. Y. Zhu, R. Paniagua-Domínguez, Y. H. Fu, B. Luk'yanchuk, A. I. Kuznetsov, "High-transmission dielectric metasurface with  $2\pi$  phase control at visible wavelengths." *Laser Photon. Rev.* 9, 412–418 (2015).
- [54] Y. Yang, W. Wang, P. Moitra, I. I. Kravchenko, D. P. Briggs, J. Valentine, "Dielectric meta-reflectarray for broadband linear polarization conversion and optical vortex generation." *Nano Lett.* 14, 1394–1399 (2014).
- [55] P. R. West, J. L. Stewart, A. V. Kildishev, V. M. Shalaev, V. V. Shkunov, F. Strohkendl, Y. A. Zakharenkov, R. K. Dodds, R. Byren, "All-dielectric subwavelength metasurface focusing lens." *Opt. Express* 22, 26212–26221 (2014).
- [56] L. Hsu, T. Lepetit, B. Kanté, "Extremely thin dielectric metasurface for carpet cloaking." arXiv preprint arXiv1503.08486 (2015).
- [57] N. I. Zheludev, "A roadmap for metamaterials." *Opt. Photon. News* 22, 30-35 (2011).
- [58] N. I. Zheludev, Y. S. Kivshar, "From metamaterials to metadevices." *Nat. Mater.* 11, 917–924 (2012).

